



**Measurement of the ratio of differential cross sections
 $\sigma(p\bar{p} \rightarrow Z + b \text{ jet})/\sigma(p\bar{p} \rightarrow Z + \text{jet})$ in $p\bar{p}$ collisions at $\sqrt{s} = 1.96$ TeV**

The DØ Collaboration
URL <http://www-d0.fnal.gov>
(Dated: November 12, 2012)

We measure the ratio of cross sections, $\sigma(p\bar{p} \rightarrow Z + b)/\sigma(p\bar{p} \rightarrow Z + j)$, for associated production of a Z boson with jets as a function of the jet transverse momentum, jet pseudorapidity, Z boson transverse momentum, and the azimuthal angle between the Z boson and jet for events with at least one b jet candidate with a $p_T > 20$ GeV and $|\eta| < 2.5$. These measurements use data collected by the DØ experiment in Run II of the Tevatron $p\bar{p}$ collisions at a center-of-mass energy of 1.96 TeV, and correspond to an integrated luminosity of 9.7 fb^{-1} . Our results are compared to predictions from next-to-leading order calculations and various Monte Carlo event generators.

Preliminary Results for HCP Conference

I. INTRODUCTION

Studies of Z boson production in association with b jets provide important tests of perturbative quantum chromodynamics (pQCD) predictions [1]. A good theoretical description of this process is essential since it forms a major background for a variety of physics processes, including the standard model (SM) Higgs boson production in association with a Z boson, $ZH(H \rightarrow b\bar{b})$ [2], and searches for supersymmetric partners of the b quark [3]. Furthermore, $Z+b$ production can serve as a reference process for non-SM Higgs boson (h) production in association with b quarks. Two different approaches are currently available to calculate Z or h boson production in association with a b quark at the next-to-leading order (NLO) [1, 4] and they yield consistent results within their respective theoretical uncertainties [5].

Both the CDF [6] and D0 [7, 8] collaborations have previously measured the ratio of the inclusive $Z+b$ jet to Z +jets production cross sections based on a fraction of the data collected in Run II of the Tevatron. Within experimental uncertainties, the obtained results agree with each other and with the theoretical predictions.

The current measurement is based on the data sample collected by the D0 experiment [9] in Run II of Fermilab's Tevatron $p\bar{p}$ collider running at a center-of-mass energy of 1.96 TeV, and corresponds to an integrated luminosity of 9.7 fb^{-1} . The enlarged data sample enables the measurement of the cross section ratio, $\sigma(Z+b)/\sigma(Z+j)$, to be performed differentially as a function of various kinematic variables. Z bosons are required to decay to pairs of leptons, $\mu\mu$ or ee , and pass at least one of the single electron or muon triggers. For our selection these triggers have an efficiency of approximately 100% for $Z \rightarrow ee$ and more than 78% for $Z \rightarrow \mu\mu$ decays depending on the transverse momentum of the muon. In addition, each event must contain at least one b jet, as identified by the standard D0 b -tagging algorithm [10]. We stress that the measurement of the ratio of cross sections benefits from the cancellation of many systematic uncertainties associated with the identification of leptons, jets, measurement of the luminosity, etc., and therefore allows for a more precise comparison of data with various theoretical predictions.

The analysis relies on all components of the D0 detector: tracking, calorimetry, muon reconstruction and the ability to identify secondary vertices. The D0 detector [9] consists of a central tracking system, comprising a silicon microstrip tracker (SMT) and a central fiber tracker, both located within a 2 T solenoidal magnet; a liquid-argon sampling calorimeter divided into a central calorimeter (CC) and two endcap calorimeters (EC) with four electromagnetic (EM) and four to five hadronic sections in depth; and a muon system consisting of three layers of tracking detectors and scintillation trigger counters. A precise reconstruction of the primary $p\bar{p}$ interaction vertex and secondary vertices are facilitated by the SMT; it also enables an accurate determination of the impact parameter defined as a distance of closest approach of the track to the interaction vertex. The impact parameter measurements of tracks, along with the secondary vertices, are an important part of the b -tagging algorithm and the discriminant used to extract the b jet content of the selected events.

II. EVENT SELECTION

An event is selected if it contains an interaction vertex, built from at least three tracks, located within 60 cm of the center of the D0 detector along the beam axis. The selected events must contain a Z boson candidate with a dilepton invariant mass $70 \text{ GeV} < m_{\ell\ell} < 110 \text{ GeV}$ ($\ell = e, \mu$).

Dielectron (ee) events are required to have two electrons of transverse momentum $p_T > 15 \text{ GeV}$ identified through electromagnetic (EM) showers in either of the two pseudorapidity [11] regions of the calorimeter: central (CC, $|\eta| < 1.1$) or endcap (EC, $1.5 < |\eta| < 2.5$). The showers must have more than 90% of their energy deposited in the EM calorimeter, be isolated from other energy depositions, and have a transverse and longitudinal profile consistent with that expected for an electron. Electron candidates in the CC region are also required to match central tracks or to produce a pattern of hits consistent with the passage of an electron through the central tracker.

Dimuon ($\mu\mu$) events are required to have two oppositely-charged muons detected in the muon spectrometer that are matched to central tracks with $p_T > 10 \text{ GeV}$ and $|\eta| < 2$. At least one muon is required to have $p_T > 15 \text{ GeV}$. These muons must pass a combined tracking and calorimeter isolation requirements. Muons originating from cosmic rays are rejected by applying timing criteria using the hits in the scintillator layers and by limiting the measured displacement of the muon track with respect to the interaction vertex.

A total of 1,249,911 Z boson candidate events are retained in the combined ee and $\mu\mu$ channels with the above criteria. The Z +jet sample is then selected by requiring at least one jet in the event with $p_T > 20 \text{ GeV}$ and $|\eta| < 2.5$. Jets are reconstructed from energy deposits in the calorimeter using an iterative midpoint cone algorithm [12] with a cone of radius $\Delta R = \sqrt{\Delta\varphi^2 + \Delta y^2} = 0.5$ where φ is the azimuthal angle and y is the rapidity. Jet energy is corrected for detector response, the presence of noise, multiple $p\bar{p}$ interactions, and energy deposited outside of the jet cone used for reconstruction.

To suppress background from top production, events are rejected if the missing transverse energy is larger than 60 GeV, reducing the $t\bar{t}$ contribution by half. These selection criteria retain an inclusive sample of 180,122 Z +jet

event candidates in the combined ee and $\mu\mu$ channels.

III. MODELING OF EVENTS

Other processes, such as diboson (WW , WZ , ZZ) production, can also contribute to the background when two leptons are reconstructed in the final state. Inclusive diboson production is simulated with the PYTHIA [13] Monte Carlo (MC) event generator. The Z +jets, including heavy flavor jets, and $t\bar{t}$ events are modeled by ALPGEN [14], to generate hard sub-processes, interfaced with PYTHIA for parton showering and hadronization. The CTEQ6L1 [15] parton distribution functions (PDFs) are used in all simulations. The cross sections of the simulated samples are then scaled to the corresponding higher order theoretical calculations. For the diboson and Z +jets processes, including $Z + b\bar{b}$ and $Z + c\bar{c}$ production, next-to-leading order (NLO) cross section predictions are taken from MCFM [16], while the $t\bar{t}$ cross section is determined from the next-to-NLO calculations of Ref. [17]. To improve the modeling of the p_T distribution of the Z boson, simulated Z +jets events are reweighted to be consistent with the measured p_T spectrum of Z bosons observed in our data [18].

These generated samples are processed through a detailed detector simulation based on GEANT [19], and are subsequently reconstructed using the same algorithms as used for real data. To model the effects of detector noise and pile-up events, collider data from random beam crossings are superimposed on simulated events. Various scale factors are applied to account for differences in reconstruction efficiency between data and simulation. The energies of simulated jets are corrected to reproduce the resolution and energy scale observed in data [20]. Jets containing b quarks have a somewhat lower energy response compared to light and c quark jets, and therefore receive an additional p_T dependent energy scale correction (at most 5% for $p_T < 30$ GeV) that is determined from simulation. In the following, light quark flavor (u , d , s) and gluon jets are referred to as “light jets” or “LF”.

The remaining contribution from multijet instrumental background events, in which jets are misidentified as leptons, is evaluated from data. This is done using a multijet-enriched sample of events that pass all selection criteria except for some of the lepton quality requirements. In the case of electrons, the multijet sample is obtained by inverting the shower shape requirement and relaxing other electron identification criteria, while for the $\mu\mu$ channel, the multijet sample consists of events with muon candidates that fail the isolation requirements. The normalization of the multijet background is adjusted by a scale factor determined from a simultaneous fit to the dilepton invariant mass distributions in the different jet multiplicity bins.

Figure 1 shows, as an example, the leading jet p_T distribution in data compared with the expectations from various processes. The dominant contribution comes from Z +light jet production. The background fraction in the ee channel is about 9.6%, and is dominated by multijet production. The muon channel has a higher purity with a background fraction of less than 1.3%.

IV. HEAVY FLAVOR ENRICHMENT

This analysis employs a two step procedure to determine the b quark content of jets in the selected events. First, a b -tagging algorithm is applied to jets in order to select a sample of Z +jets events that is enriched by heavy flavor jets. After b -tagging, the relative light, charm, and b quark content of events is extracted by fitting the templates built from a dedicated discriminant which provides an optimized separation between the three components.

Jets considered for b -tagging are subject to a preselection requirement, called taggability, to decouple the intrinsic b -jet tagging algorithm performance from effects related to track reconstruction inefficiency. For this purpose, the jet is required to have at least two associated tracks with $p_T > 0.5$ GeV, the leading track must have $p_T > 1$ GeV, and each track must have at least one SMT hit. This requirement has a typical efficiency of 90% per jet.

The b -tagging algorithm is based on a multivariate analysis (MVA) technique [21]. This algorithm, known as the MVA_{bl} since it discriminates b -like jets from LF-like jets, utilizes the relatively long lifetime of the b hadrons when compared to their lighter counterparts [10]. Events are considered to be b -tagged if the leading or sub-leading jet is tagged by this algorithm.

The MVA_{bl} discriminant combines various properties of the jet and associated tracks to create a continuous output which tends towards unity for b jets and zero for light jets. The input variables include the number of reconstructed secondary vertices in the jet, the invariant mass of the charged particles associated with the secondary vertex (secondary vertex mass, M_{SV}), the number of tracks in the reconstructed secondary vertex, the decay length significance of the secondary vertex, defined as the transverse decay length divided by its uncertainty, the weighted sum of the transverse impact parameter significance of tracks, and the Jet Lifetime Probability (JLIP) which is a probability that tracks associated with the jet originate from the interaction vertex. Events are retained for further analysis if they contain at least one jet with an MVA_{bl} output greater than 0.1 and a valid secondary vertex mass; the latter assumes

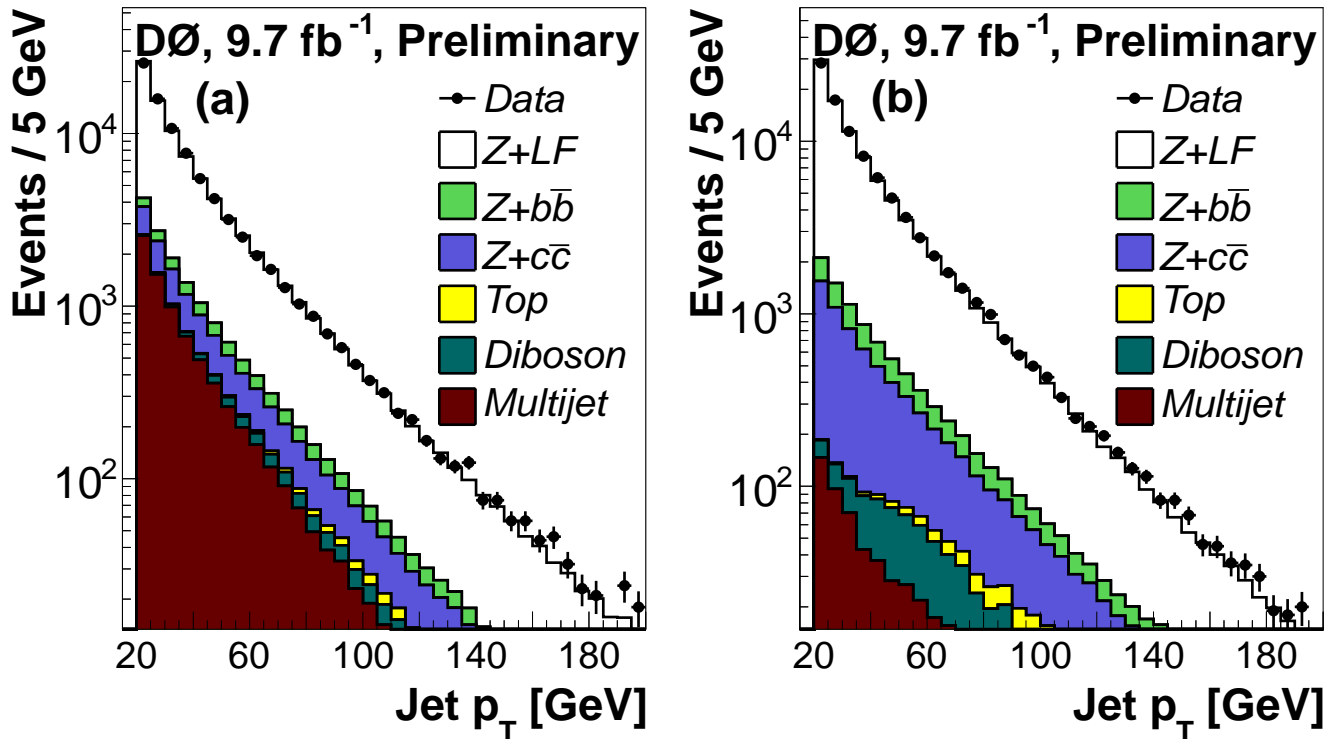


FIG. 1: (color online) The leading jet p_T in the (a) $Z \rightarrow ee$ and (b) $Z \rightarrow \mu\mu$ channels for data and background in the $Z + \geq 1$ jets sample before any b -tagging is applied.

that a secondary vertex can be associated with the jet. After these requirements, a total of 4,114 Z +jets events are selected with at least one b -tagged jet. The efficiency for tagging b , c and light jets are approximately 40%, 10% and 0.4%, respectively, depending on jet p_T and η . The resulting background contamination from diboson, multijet, and top production after b -tagging, for the electron and muon channel, is 10.4% and 4.8%, respectively.

V. EXTRACTION OF FLAVOR FRACTIONS

To determine the fraction of events with b , c and light jets, a dedicated discriminant, D_{MJL} , is employed [8]. It is a combination of the two most discriminating variables mentioned above, M_{SV} and JLIP: $D_{\text{MJL}} = 0.5 \times (M_{\text{SV}}/5 \text{ GeV} - \ln(\text{JLIP})/20)$. The coefficients in this equation are chosen empirically to ensure that the bulk of the D_{MJL} values fall between 0 and 1. Figure 2 shows the D_{MJL} distributions, used as templates, obtained from simulations of all three considered jet flavors that pass the b -tagging requirement. Also shown in Fig. 2 is the corresponding distribution for a light jet enriched data sample, known as negatively tagged jets. These jets have negative values for some of the inputs for the MVA_{bl} algorithm, such as decay length significance and impact parameter, which are caused by the detector resolution effects. We estimate the b jet contamination in the negatively tagged data using a maximum likelihood fit and subtract its contribution. A small difference in the shape of the templates as measured in the negatively tagged and MC light jet samples is taken as a systematic uncertainty.

To measure the fraction of events with different jet flavors in the final selected sample, we perform a binned maximum likelihood fit to the D_{MJL} distribution in data using the b , c , and light flavor jet templates. Before the fit, all non- $(Z+\text{jet})$ background contributions estimated after the MVA_{bl} requirement, i.e., multijet, diboson and $t\bar{t}$, are subtracted from the data leaving 1,854 and 1,946 Z +jet events in the ee and $\mu\mu$ channels, respectively. Next, we measure the jet flavor fractions in the dielectron and dimuon samples separately, yielding the b jet flavor fractions of 0.284 ± 0.028 (stat.) and 0.333 ± 0.026 (stat.), respectively. Since these measurements are in agreement, within their statistical uncertainties, we combine the two samples in order to increase the statistical power of the fit for individual jet flavors. The measured fractions of b , c , and light flavor jets are 0.300 ± 0.019 (stat.), 0.375 ± 0.035 (stat.), and 0.325 ± 0.025 (stat.), respectively. The combined D_{MJL} distribution of the b -tagged data and the fitted templates for the b , c and light jets are shown in Fig. 2.

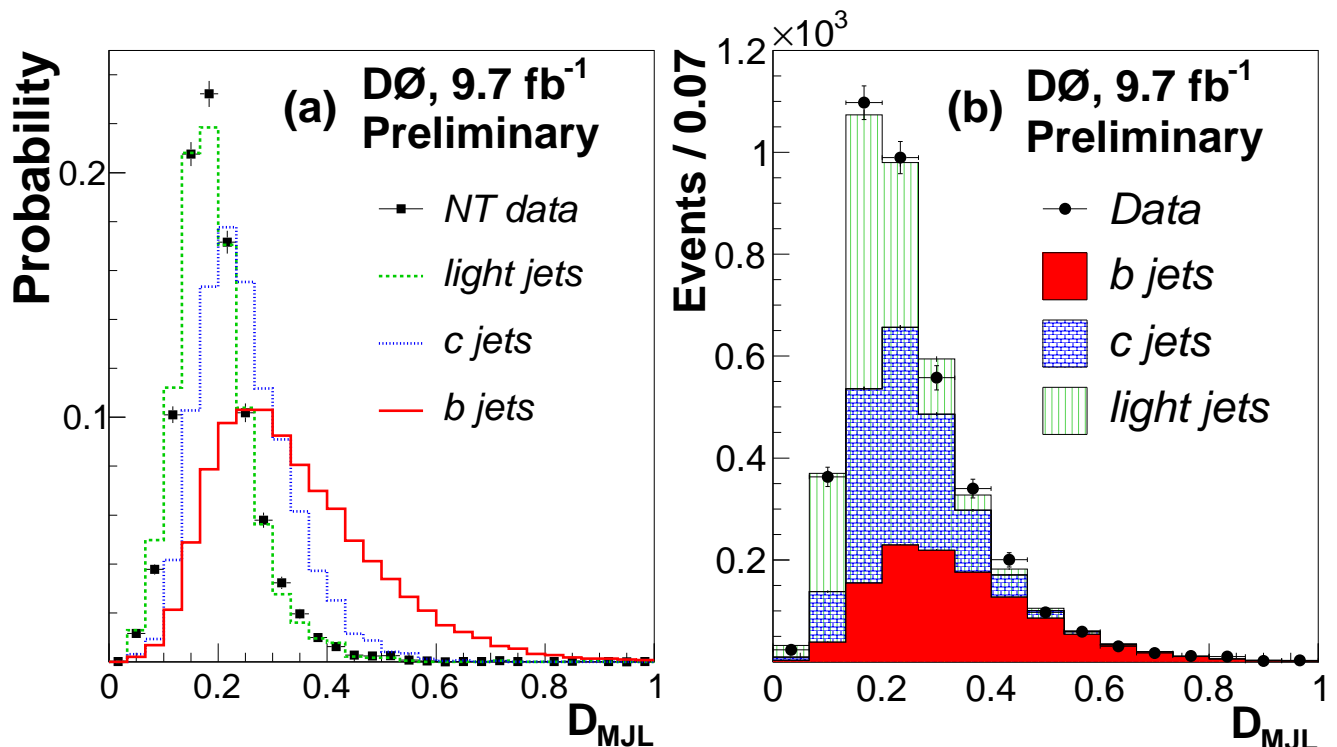


FIG. 2: (color online) a) The probability densities of the D_{MJL} discriminant for b , c , and light jets passing the b -tagging requirements. These templates are taken from MC. Also shown is the distribution for the negatively tagged jets in data, described in the text. b) The D_{MJL} discriminant distribution of events in the combined sample. The distributions of the b , c , and light jets are weighted by the fractions found from the fit. Uncertainties are statistical only.

VI. MEASUREMENT OF THE CROSS SECTION RATIO

The measured fractions of b , c , and light jets in the selected sample of Z +jet event candidates can now be combined with the corresponding acceptances of events, estimated using simulations, and the ratio of cross sections can be determined using the following equation:

$$\frac{\sigma(Z+b)}{\sigma(Z+j)} = \frac{N f_b}{N_{\text{incl}} \epsilon_{\text{tag}}^b} \times \frac{\mathcal{A}_{\text{incl}}}{\mathcal{A}_b} \quad (1)$$

where N_{incl} is the total number of Z +jet events before any tagging requirement, N is the number of Z +jet events used in the D_{MJL} fit, f_b is the b jet fraction, and ϵ_{tag}^b is the overall D_{MJL} efficiency for b jets which combines the efficiencies for taggability, MVA_{bl} discriminant and D_{MJL} selection. Both N_{incl} and N correspond to the number of events that remain after the non- Z +jet processes have been subtracted from the data.

The detector acceptances for the inclusive sample, $\mathcal{A}_{\text{incl}}$, and b jets, \mathcal{A}_b , are determined from simulations. The corresponding events are generated with ALPGEN in the kinematic region that satisfy p_T and η requirements for leptons and jets. The resulting ratio of the two acceptances is measured to be $\mathcal{A}_{\text{incl}}/\mathcal{A}_b = 1.12 \pm 0.002$ (stat.). In this ratio, the effect of migration of events near the kinematic threshold, or neighboring kinematic bins, due to the finite detector resolution is found to be negligibly small.

The result for the ratio of the $Z+b$ cross section to the inclusive Z +jet cross section in combined $\mu\mu$ and ee channels, including the systematic uncertainty which is discussed in the following section, is 0.0202 ± 0.0014 (stat.) ± 0.0018 (syst.). This measurement is in agreement with the previous D0 result of 0.0193 ± 0.0027 [8] and the NLO pQCD prediction of $0.0206^{+0.0022}_{-0.0013}$ [1] which is corrected for non-perturbative effects as discussed in Sec. VIII.

We now proceed with the measurement of the $\sigma(Z+b)/\sigma(Z+j)$ differential cross section ratio as a function of various kinematic quantities. The following four variables have been considered: jet p_T , jet η , Z boson p_T , and $\Delta\varphi_{Z,\text{jet}}$ – azimuthal angle between the Z boson and the closest jet in the event. The data are split into five bins for

TABLE I: Final results for the ratio of differential cross sections, $\sigma(Z + b)/\sigma(Z + j)$, in various bins of jet p_T , jet η , Z boson p_T , and $\Delta\varphi_{Z,\text{jet}}$.

Jet p_T [GeV]	N [Events]	$\frac{\sigma(Z+b)}{\sigma(Z+j)}$	Statistical Uncertainty	Systematic Uncertainty
20 – 30	1317	0.0175	0.0010	0.0022
30 – 40	858	0.0192	0.0012	0.0019
40 – 55	712	0.0210	0.0016	0.0015
55 – 70	369	0.0231	0.0025	0.0021
70 – 200	535	0.0226	0.0033	0.0022
<hr/>				
Z p_T [GeV]				
0 – 20	502	0.0283	0.0029	0.0050
20 – 40	1326	0.0112	0.0007	0.0010
40 – 60	998	0.0200	0.0011	0.0012
60 – 80	512	0.0236	0.0018	0.0016
80 – 200	453	0.0334	0.0034	0.0025
<hr/>				
Jet η				
0 – 0.25	614	0.0131	0.0012	0.0010
0.25 – 0.5	639	0.0164	0.0014	0.0012
0.5 – 1.0	1180	0.0209	0.0010	0.0018
1.0 – 1.5	888	0.0213	0.0014	0.0027
1.5 – 2.5	477	0.0152	0.0017	0.0027
<hr/>				
$\Delta\varphi_{Z,\text{jet}}$ [Rad]				
0 – 2.5	833	0.0292	0.0019	0.0040
2.5 – 2.75	514	0.0212	0.0024	0.0023
2.75 – 2.9	596	0.0215	0.0015	0.0020
2.9 – 3.05	961	0.0151	0.0009	0.0012
3.05 – 3.2	895	0.0131	0.0010	0.0009

each variable such that the sample sizes allow for a stable fit with the D_{MJL} templates. The templates, in turn, are constructed individually for every bin and each examined variable. The selected bin sizes along with the corresponding statistics of data events used in the fit are listed in Table I. In each case, all the quantities that enter into Eq. (1) are remeasured separately. A summary of the differential cross section ratio measurements can also be found in Table I.

VII. SYSTEMATIC UNCERTAINTIES

Various systematic uncertainties cancel when the ratio of cross sections, $\sigma(Z + b \text{ jet})/\sigma(Z + \text{jet})$, is measured. These include uncertainties on the luminosity measurement, trigger, lepton, and some of the jet identification efficiencies. The remaining uncertainties are estimated for the integrated result and in each bin of the examined variable and bin separately. For the integrated result, the largest systematic uncertainty of 7.6% is due to the b jet energy calibration; it is comprised of the uncertainties on the jet energy resolution and the jet energy scale. The next largest systematic uncertainty of 3.9% comes from the shape of the D_{MJL} templates used in the fit. A variety of different aspects can affect the shape of the templates, including the choice of the b quark fragmentation function, the background estimation, the difference in the shape of the light jet MC and negatively tagged data templates, and the uncertainty from the fit itself. These are all evaluated by varying the central values by the corresponding uncertainties, one at a time, and repeating the entire analysis chain. The other sources of uncertainties are due to the b jet identification efficiency (1.8%) and the choice of the MC event generator, ALPGEN vs SHERPA [23], for the detector acceptance evaluations ($< 0.1\%$). For the integrated ratio measurement, these uncertainties results in a total systematic uncertainty of 8.7%. The corresponding total systematic uncertainties for the ratios of differential cross sections are listed in Table I while Table II lists them separately for each variable and bin.

VIII. COMPARISON TO PREDICTIONS

The measurements are compared to predictions from an NLO pQCD calculation and two leading order MC event generators, SHERPA and ALPGEN.

The NLO predictions are based on MCFM [1], version 5.6, with the MSTW2008 PDFs [22] and the renormalization and factorization scales set at $Q_R^2 = Q_F^2 = m_Z^2 + \sum p_{T,\text{jet}}^2$; here m_Z is the Z boson mass and $p_{T,\text{jet}}$ is the transverse

TABLE II: Systematic uncertainties, in percentage, for the ratio of differential cross sections.

Source of Systematic	Uncertainty [%]					
	Jet p_T [GeV]	20 – 30	30 – 40	40 – 55	55 – 70	70 – 200
Jet Energy Scale, Resolution		10.7	7.4	4.3	4.9	2.6
Template Shape		5.7	4.9	5.1	6.3	6.8
b-ID		1.2	1.4	1.9	2.5	2.6
Acceptance		3.3	3.4	0.4	3.2	5.9
Jet η		0 – 0.25	0.25 – 0.5	0.5 – 1.0	1.0 – 1.5	1.5 – 2.5
Jet Energy Scale, Resolution		4.3	4.0	5.8	9.6	12.9
Template Shape		5.9	5.5	5.3	5.9	6.9
b-ID		1.3	1.3	1.4	1.5	5.7
Acceptance		1.5	2.2	2.7	5.1	8.6
Z p_T [GeV]		0 – 20	20 – 40	40 – 60	60 – 80	80 – 200
Jet Energy Scale, Resolution		16.4	5.7	2.0	0.8	1.5
Template Shape		6.1	4.8	5.1	6.2	6.4
b-ID		1.6	1.7	1.8	1.9	2.1
Acceptance		1.1	4.8	0.2	1.8	3.2
$\Delta\varphi_{Z,\text{jet}}$ [Rad]		0 – 2.5	2.5 – 2.75	2.75 – 2.9	2.9 – 3.05	3.05 – 3.2
Jet Energy Scale, Resolution		11.5	8.8	6.6	5.3	3.8
Template Shape		6.6	5.6	5.5	4.8	4.9
b-ID		1.7	1.8	2.0	2.0	1.9
Acceptance		3.1	2.5	2.2	1.9	1.8

momentum of the jet. Corrections are applied to the MCFM predictions to account for non-perturbative effects that are estimated using ALPGEN. Uncertainties on the theoretical predictions are evaluated by simultaneously changing the renormalization and factorization scales up or down by a factor of two.

The ratio of differential cross sections as a function of jet p_T , η , Z boson p_T , and $\Delta\varphi_{Z,\text{jet}}$ are compared to predictions from MCFM, ALPGEN, and SHERPA in Fig. 3. None of the predictions can fully describe all the examined variables, except for the jet p_T . Overall, within the current experimental and theoretical uncertainties, the data are better described by NLO predictions, while dependence on the Z boson p_T is best described by ALPGEN and the $\Delta\varphi_{Z,\text{jet}}$ correlation by SHERPA.

IX. CONCLUSIONS

We measure the integrated cross section ratio, $\sigma(p\bar{p} \rightarrow Z + b)/\sigma(p\bar{p} \rightarrow Z + j)$, as well as the ratio of the differential cross sections in bins of jet p_T , jet η , Z boson p_T , and $\Delta\varphi_{Z,\text{jet}}$, for events with $Z \rightarrow \ell^+\ell^-$ ($\ell = e, \mu$) candidates and at least one b jet in the final state. Measurements are based on the full data sample collected by the D0 experiment in Run II of the Tevatron, corresponding to an integrated luminosity of 9.7 fb^{-1} at a center-of-mass energy of 1.96 TeV. For jets with transverse momentum $p_T > 20 \text{ GeV}$ in pseudorapidity $|\eta| < 2.5$, the measured integrated ratio of 0.0202 ± 0.0014 (stat.) ± 0.0018 (syst.) which is in agreement with NLO pQCD predictions. Results for the ratio of differential cross sections are also compared to predictions from two Monte Carlo event generators. These generally show poor agreement with the data in at least one variable.

We thank the authors of Refs. [1, 5, 23] for valuable discussions, and the staffs at Fermilab, and collaborating institutions, and acknowledge support from the DOE and NSF (USA); CEA and CNRS/IN2P3 (France); MON, NRC KI and RFBR (Russia); CNPq, FAPERJ, FAPESP and FUNDUNESP (Brazil); DAE and DST (India); Colciencias (Colombia); CONACyT (Mexico); NRF (Korea); FOM (The Netherlands); STFC and the Royal Society (United Kingdom); MSMT and GACR (Czech Republic); BMBF and DFG (Germany); SFI (Ireland); The Swedish Research Council (Sweden); and CAS and CNSF (China).

-
- [1] J. M. Campbell, R. K. Ellis, F. Maltoni, and S. Willenbrock, Phys. Rev. D **69**, 074021 (2004).
[2] V. M. Abazov *et al.* (D0 Collaboration), Phys. Rev. Lett. **104**, 071801 (2010); arXiv:hep-ex/1008.3564; T. Aaltonen *et al.* (CDF Collaboration), Phys. Rev. D **80**, 071101 (2009); arXiv:hep-ex/1009.3047.
[3] V. M. Abazov *et al.* (D0 Collaboration), Phys. Lett. B **693**, 95 (2010); T. Aaltonen *et al.* (CDF Collaboration), Phys. Rev. Lett. **105**, 081802 (2010).

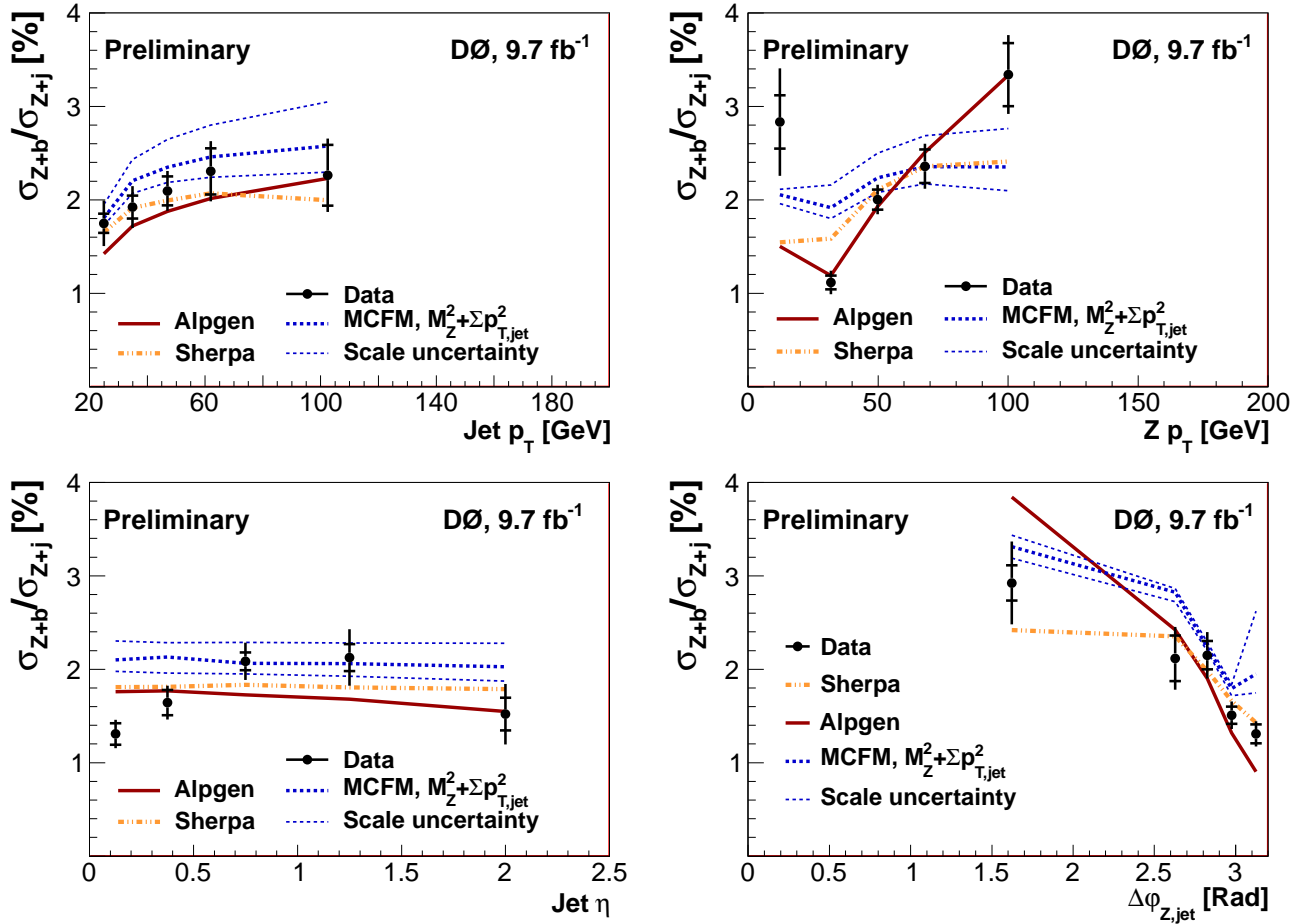


FIG. 3: (color online) Ratios of the differential cross sections for jets with $p_T > 20$ GeV and $|\eta| < 2.5$. The uncertainties on the data include statistical (inner error bar) and full uncertainties (entire error bar). The solid red line shows the prediction from ALPGEN, the dash-dotted orange line is from SHERPA, and the blue dotted lines are for the MCFM NLO, where the thick line corresponds to the central scale choice and the band represents the variation of the scale up and down by a factor of two. Bin centers are chosen using the prescription found in Ref. [27]

- [4] F. F. Cordero, L. Reina, and D. Wackerath, Phys. Rev. D **78**, 074014 (2008).
- [5] S. Dawson, C. B. Jackson, L. Reina, and D. Wackerath, Modern Phys. Lett. A **21**, 89 (2006).
- [6] T. Aaltonen *et al.* (CDF Collaboration), Phys. Rev. D **79**, 052008 (2009).
- [7] V. M. Abazov *et al.* (D0 Collaboration), Phys. Rev. Lett. **94**, 161801 (2005).
- [8] V. M. Abazov *et al.* (D0 Collaboration), Phys. Rev. D **83**, 031105 (2011).
- [9] V.M. Abazov *et al.* (D0 Collaboration), Nucl. Instrum. Methods Phys. Res. A **565**, 463 (2006); M. Abolins *et al.*, Nucl. Instrum. Methods Phys. Res. A **584**, 75 (2008); R. Angstadt *et al.*, Nucl. Instrum. Methods Phys. Res. A **622**, 298 (2010).
- [10] V. M. Abazov *et al.* (D0 Collaboration), Nucl. Instrum. Methods Phys. Res. Sect. A **620**, 490 (2010).
- [11] Pseudorapidity $\eta = -\ln[\tan(\theta/2)]$ with polar angle θ measured relative to the proton beam direction.
- [12] G. C. Blazey *et al.*, arXiv:hep-ex/0005012.
- [13] T. Sjöstrand, S. Mrenna, and P. Skands, J. High Energy Phys. **05**, 026 (2006). Version 6.409 with Tune A was used.
- [14] M. L. Mangano *et al.*, J. High Energy Phys. **07**, 001 (2003). Version 2.11 was used.
- [15] J. Pumplin *et al.*, J. High Energy Phys. **07**, 012 (2002).
- [16] J. M. Campbell and R. K. Ellis, Phys. Rev. D **60**, 113006 (1999); *ibid.* **62**, 114012 (2000); *ibid.* **65**, 113007 (2002).
- [17] U. Langenfeld, S. Moch, and P. Uwer, Phys. Rev. D **80**, 054009 (2009).
- [18] V. M. Abazov *et al.* (D0 Collaboration), Phys. Rev. Lett. **100**, 102002 (2008).
- [19] R. Brun and F. Carminati, CERN Program Library Long Writeup W5013 (1993).
- [20] V. M. Abazov *et al.* (D0 Collaboration), Phys. Rev. D **85**, 052006 (2012).
- [21] Andreas Hoecker, Peter Speckmayer, Joerg Stelzer, Jan Therhaag, Eckhard von Toerne, and Helge Voss. TMVA: Toolkit for Multivariate Data Analysis. PoS, ACAT:040, 2007.
- [22] A. D. Martin, W. J. Stirling, R. S. Thorne, and G. Watt, Eur. Phys. J. C **63**, 189 (2009).

- [23] T. Gleisberg *et al.*, J. High Energy Phys. **02**, 007 (2009).
- [24] W.K. Tung *et al.*, J. High Energy Phys. **02**, 052 (2007).
- [25] S. Catani *et al.*, J. High Energy Phys. **11**, 063 (2001).
- [26] F. Caravaglios *et al.*, Nucl. Phys. B539, **215** (1999).
- [27] G.D. Lafferty, T.R. Wyatt, Nucl. Instrum. Methods Phys. Res. Sect. A **355**, 541 (1995).